energies

MDPI

Article

An Adaptive Phase Locked Oscillator to Improve the Performance of Fault Recovery from Commutation Failure in LCC-Based HVDC Systems

Hongda Cai [1,†], Jing Li [1,†], Yongzhi Zhou [2,*,†] and Yishuang Hu [1,†]

[1] School of Information and Electrical Engineering, Hangzhou City University, Hangzhou 310015, China; caihd@zucc.edu.cn (H.C.); huys@zucc.edu.cn (Y.H.)
[2] Polytechnic Institute, Zhejiang University, Hangzhou 310015, China
* Correspondence: zhouyongzhi@zju.edu.cn
† These authors contributed equally to this work.

Abstract: An adaptive control of phase lock oscillator (PLO) is proposed to increase the ability of LCC-based HVDC systems to successfully recover from commutation failure, where the dynamic performance during the recovery process is improved. The phase lock oscillator is one of the most important parts of the control system, which is used to trace the phase angle of commutating voltage. However, the PLO with constant parameters cannot provide accurate information under both steady-state operation and large disturbances. In our work, the control parameters of PLO can be adaptively adjusted, following the states of commutating voltage. When the system is operating in a steady state, the PLO selects parameters that exhibit improved small-signal stability, while parameters prioritizing dynamic behaviors with high-tracing accuracy are adopted during large disturbances. Case studies based on simulations in PSCAD/EMTDC and RT-LAB show that the proposed control strategy can improve the performance of fault recovery from CF.

Keywords: commutation failures; phase lock oscillator; recovery from commutation failure; LCC-based HVDC systems

Citation: Cai, H.; Li, J.; Zhou, Y.; Hu, Y. An Adaptive Phase Locked Oscillator to Improve the Performance of Fault Recovery from Commutation Failure in LCC-Based HVDC Systems. *Energies* **2023**, *16*, 5299. https://doi.org/10.3390/en16145299

Academic Editor: Sérgio Cruz

Received: 22 May 2023
Revised: 20 June 2023
Accepted: 1 July 2023
Published: 11 July 2023

1. Introduction

Commutation failures (CFs) are very common events in traditional line commutated converter (LCC)-based HVDC systems, which are usually caused by voltage reductions following AC-side faults [1–3]. The occurrence of CF will inevitably cause many transients, such as temporary interruption of power transmission, voltage fluctuation, etc. [4,5]. After the fault is cleared, the HVDC system is expected to recover from CF as soon as possible. Otherwise, continuous CFs may cause converter block [6], which threatens system security. It is important to improve the recovery performance to counter continuous CFs, and many previous works have been dedicated to this topic [7–9].

For LCC-based HVDC systems, the valve-firing control system generates valve-firing pulses, based on the firing angle order and the reference voltage at the AC side. The control system plays the most important role during the transient of recovery from CF. Currently, the most widely implemented control strategies in the real world can be categorized into either an ABB-based or SIEMENS-based strategy. For the two types of control strategies, the calculations of the firing angle order are different, but the key idea of the control system during the transient is very similar, which is to enlarge the margin of extinction angle by triggering the thyristor gates in advance. Many auxiliary controls have been proposed to improve the performance under large disturbances [10,11], among which the commutation failure prevention (CFPREV) mechanism has been widely applied [12]. In addition, many different types of dynamic var sources have been used to enhance the immunity against CFs, e.g., synchronous compensator (SC), static synchronous compensator (STATCOM) [13,14], etc.

In the previous literature, the main focus is centered on inducing the firing angle order, which will then be fed into the firing pulse generator to create trigger pulses. Usually, the firing pulses are generated by comparing the firing angle order and the measured commutating voltage phase angle. The dynamic behavior of the phase angle measurement will definitely influence the performance of recovery from CF, which has attracted many researchers. Authors in [15] compared the dynamic performance of different HVDC systems under traditional phase-lock control and PLL-less control. In ref. [16], a novel phase-locked strategy is proposed based on dynamic phasor modelling to provide more accurate phase angle information. The influence of phase-locked control on small single stability was analyzed in [17], and the results showed that there are coupling effect between phase-locked controller and LCC controller. To overcome the disadvantage of traditional phase-lock control under the unbalanced and distorted grid conditions, a double decouple synchronous reference frame was proposed in [18].

In LCC-based HVDC systems, the phase-locked oscillator (PLO) is usually applied to provide the phase information. During the transient process of recovery from CFs, the dynamic behavior of PLO will definitely influence the execution of firing thyristors. If the measured phase angle deviates from the real phase angle, the thyristors may not fire correctly, inducing unexpected CFs. In this paper, a novel adaptive PLO is proposed, where the control parameters can be adaptively changed following the system state. During the process of recovery from CF, the var consumption of converters will rise from 0 to about 60% of the active power consumption in a very short period, which will induce the fluctuation of commutating voltage. Thus, if the PLO cannot capture the voltage phase information correctly under a large signal disturbance, the recovery may fail and continuous CFs will happen.

In this paper, an adaptive PLO structure is proposed to improve the performance of recovery process from CF, where the control parameters can be adjusted following the system state. During the process of fault recovery, the PLO is preferred to capture the fast change of commutating voltage, whereas the small signal stability is considered as the more important factor during normal operation. The main contributions can be summarised as follows: the proposed PLO can improve transient performance compared to the traditional method, which can provide more accurate phase information during the fault recovery process.

The rest of this paper is organized as follows. Section 2 presents the parametric fault voltage equations and the main problems to be resolved, and then the detailed solution method is illustrated in Section 4. In Section 5, case studies are performed to demonstrate the effectiveness of the approach, followed by concluding remarks in the last section.

2. Phase-Locked Oscillator

To understand the function of PLO in LCC-based HVDC systems, a schematic is illustrated in Figure 1. As can be seen, the firing angle order to control the inverter is provided by the current/voltage/extinction angle controller, based on the measured voltage and current from both the AC and DC sides. The firing pulse generator then creates firing pulses supplied to each gate, in response to the signals of firing angle order and measured phase angle. The PLO system is used to determine the phase of commutating voltage, where phase vector techniques are applied. If the output of PLO cannot accurately reflect the phase angle of commutating voltage, the generated firing pulse may not trigger the gate as expected. During the process of system recovery from CF, the output error of PLO may cause continuous CFs.

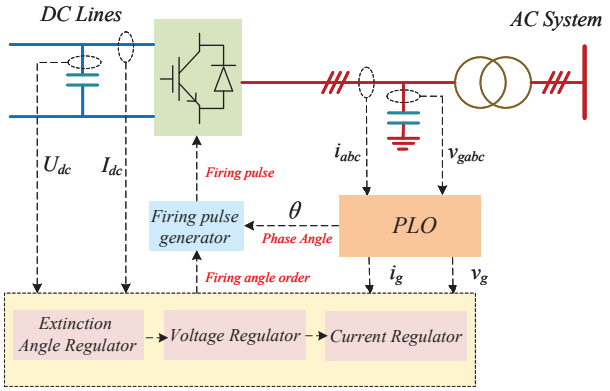

Figure 1. Diagram of control block in LCC-based HVDC systems.

2.1. Detailed Mathematical Model of PLO

Without loss of generality, we assume that the AC phase voltages are:

$$\begin{cases} u_a &= U_m \sin \omega t, \\ u_b &= U_m \sin(\omega t + \pi/3), \\ u_c &= U_m \sin(\omega t - \pi/3), \end{cases} \tag{1}$$

where U_m is the voltage magnitude of each phase. u_a, u_b and u_c are the voltage of phase-A, phase-B and phase-C, respectively. ω is the system angular frequency. Figure 2 shows the whole model of PLO. As seen, the AC-side voltage in the form of "*abc*-coordinates" is firsy transformed into the expression under "$\alpha\beta$-coordinates":

$$\begin{pmatrix} u_\alpha \\ u_\beta \end{pmatrix} = \frac{2}{3} \cdot \begin{pmatrix} 1 & -0.5 & -0.5 \\ 0 & \frac{\sqrt{3}}{2} & -\frac{\sqrt{3}}{2} \end{pmatrix} \begin{pmatrix} u_a \\ u_b \\ u_c \end{pmatrix}, \tag{2}$$

where u_a, u_b and u_c are the phase voltages of the AC system, u_α and u_β are the transformed voltages under $\alpha\beta$-coordinates.

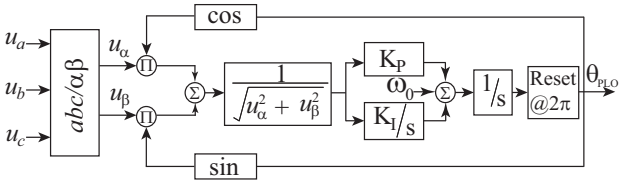

Figure 2. Control block diagram of PLO.

A correction signal of phase angle is then created and sent to a PI-controller, which can accelerate and slow down the PLO to match the voltage phase [19,20]:

$$\theta_{err} = \frac{u_\alpha \cos\theta_{PLO} + u_\beta \sin\theta_{PLO}}{\sqrt{u_\alpha^2 + u_\beta^2}}, \tag{3}$$

where θ_{PLO} is the output of PLO, and θ_{err} is the correction signal. Note that, θ_{err} should be zero when θ_{PLO} is just the phase angle of u_a.

The mathematical model of PI-controller and integrator can be expressed as

$$\begin{cases} \dot{\theta}_{tmp} &= K_I \theta_{err}, \\ \dot{\theta}_{PLO} &= K_P \theta_{err} + \theta_{tmp} + \omega_0, \end{cases} \tag{4}$$

where θ_{tmp} is the output of integrator part in the PI-controller, K_P and K_I are the proportinal and integral gains of the PI controller, ω_0 is the nominal angular speed of AC system. Hereafter, the dot just above the variable denotes that this is the variable's derivative.

At last, θ_{PLO} will be reset to 0 when θ_{PLO} reaches 2π.

2.2. Influence of PLO Tracing Error on the Process of Commutation

When the system is operating normally with no disturbance, the output of PLO is expected to be a ramp depicted as the black solid line in Figure 3, which can represent the phase angle of commutating voltage. By comparing the firing angle order with this ramp, a firing pulse can be created to trigger the corresponding gate. In this case, the maximum voltage–time area for commutation should be

$$A_{cmt} = \int_{\alpha}^{\pi} \sqrt{3} U_m \sin \omega t \, d\omega t = \sqrt{3}(1 + \cos \alpha) U_m, \tag{5}$$

where α is the firing delay angle and A_{cmt} is the maximum voltage–time area for commutation.

Assume that, there is a time lag α_ϵ between the expected and measured phase angle, shown as the black solid and red dashed lines, respectively. The firing pulse will be created with a delay angle of $\alpha + \alpha_\epsilon$, which means the maximum voltage–time area for commutation is

$$A'_{cmt} = \int_{\alpha+\alpha_\epsilon}^{\pi} \sqrt{3} U_m \sin \omega t \, d\omega t = \sqrt{3}[1 + \cos(\alpha + \alpha_\epsilon)] U_m, \tag{6}$$

where A'_{cmt} is the maximum voltage–time area for commutation considering time lag.

The deduction of voltage–time area can be evaluated:

$$\Delta A_{cmt} = A_{cmt} - A'_{cmt} = \sqrt{3}[\cos \alpha - \cos(\alpha + \alpha_\epsilon)] U_m. \tag{7}$$

From (7), it is known that the time lag of measured phase angle will reduce the maximum voltage-time area. During the recovery from CF, the unexpected reduction may cause continuous CFs. Thus, an accurate output of PLO is very essential to eliminate the continuous CFs.

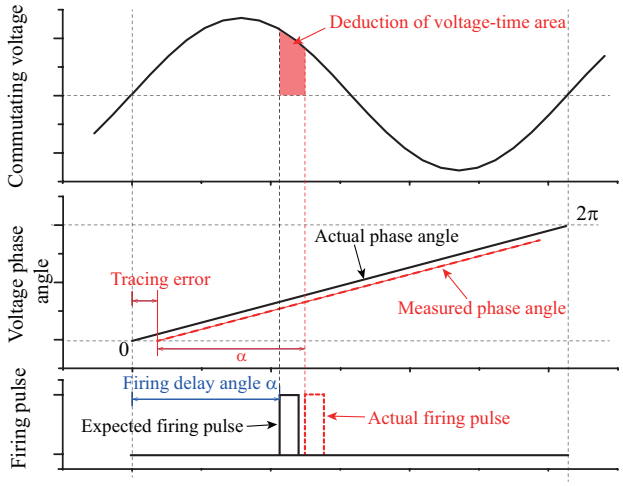

Figure 3. The deduction of voltage-time area caused by the tracing error of measured phase angle.

3. Impact of Control Parameters on Dynamic Behavior of PLO

In this section, the dynamic behavior of PLO block under different control parameters is analysed, where small signal stability and transient performance are discussed.

3.1. Small Signal Stability

From (1)–(4), the following model for analysing small signal stability of the PLO control block can be derived:

$$\begin{pmatrix} \Delta\dot{\theta}_{tmp} \\ \Delta\dot{\theta}_{PLO} \end{pmatrix} = \begin{pmatrix} 0 & -K_I \\ 1 & -K_P \end{pmatrix} \begin{pmatrix} \Delta\theta_{tmp} \\ \Delta\theta_{PLO} \end{pmatrix}, \tag{8}$$

based on which the eigenvalues of the corresponding eigen matrix are $\frac{-K_P \pm \sqrt{K_P^2 - 4K_I}}{2}$.

Figures 4 and 5 depict the real and imaginary parts of eigenvalues with different K_P and K_I, respectively. When K_P is increased, it can be seen that the real part of eigenvalues diverge into two branches at the point $K_P = 2\sqrt{K_I}$. The upper branch tends to 0, meaning that the rightmost eigenvalue moves closer to the boundary of small signal stability. From the imaginary part, it can be concluded that increasing K_P can make the eigenvalues become close to the real axis and then move on the negative real axis, with one from left to right and the other from right to left. Thus, the parameter K_P is expected to be smaller to gain higher stability, but oscillation may be observed.

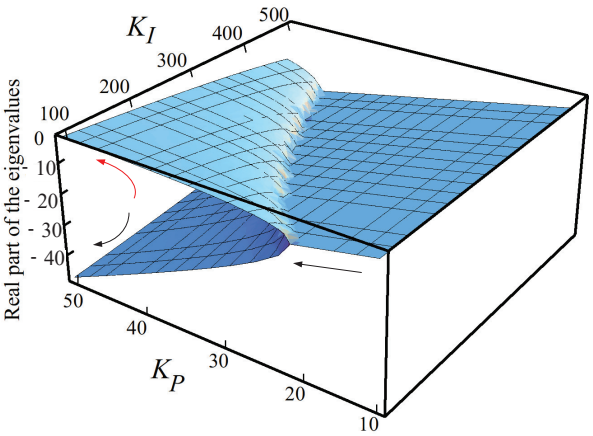

Figure 4. The real part of eigenvalues with different K_P and K_I. The arrows indicate the changing directions of the eigenvalues.

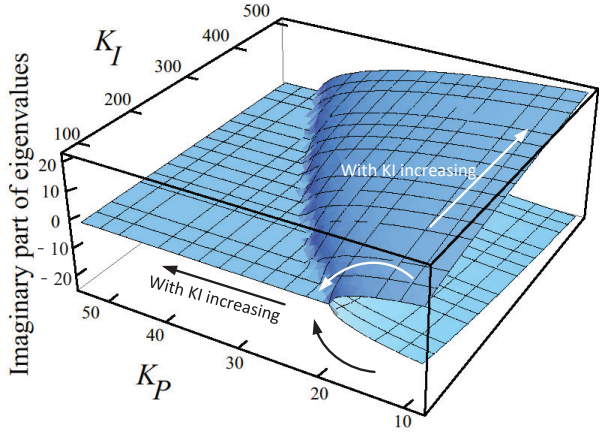

Figure 5. The imaginary part of eigenvalues with different K_P and K_I. The arrows indicate the changing directions of the eigenvalues.

If $K_P < 2\sqrt{K_I}$, increasing K_I can reduce the real part of eigenvalue. That means, it would be beneficial to increase K_I to improve the small signal stability. However, it should be noted that, larger K_I tends to have oscillation as seen from the imaginary part. Thus, the tuning of the control parameter is a tradeoff between stability and steady performance.

Combined with the aforementioned analysis, trial and error or other optimization methodology can been adopted to determine the control parameters.

3.2. Dynamic Performance in Response to a Large Disturbance

Aside from the stability under small changes, the dynamic performance in response to a disturbance is another general issue to be addressed. For the PLO, the fast response to the change of phase angle during the recovery process from CF should mainly be focused, where the PI-controller for speeding up and slowing down the PLO plays a dominant role. To gain a fast response, the adjustment of PLO should be fast enough, meaning that the control part of accelerating and slowing down should be very sensitive to θ_{err}. From (4), it can be seen that the adjustment is determined by the proportional part and the integration part of the PI-controller, and the proportional part can readily respond to θ_{err}. Thus, a K_P of larger value can make the output of PLO respond faster to the change in commutating voltage.

4. The Adaptive PLO Control Algorithm

From Section 3, it is known that the parameters of PI-controller are very important to the performance of PLO. In our work, an adaptive scheme of control parameters is proposed, where the PI-controller applies different control parameters under different conditions.

For the LCC-based HVDC systems, the commutation process highly relies on the commutating voltage, so the variation of commutating voltage is selected to indicate the system operation condition. During the CF faults at the converter side induced by AC system faults, the commutating voltage is typically at a low level. After the AC system faults are cleared, the commutating voltage begins to rise along with the recovery from CF. If the variation of commutating voltage is greater than a threshold value, it is reasonable to regard the system is suffering a large disturbance. Assume that, the rms of commutating voltage is U_{rms}. Then,

$$\begin{cases} \text{If } \dot{U}_{rms} > C_s, \text{ the system is with large disturbance,} \\ \text{If } \dot{U}_{rms} \leq C_s, \text{ the system is under steady state,} \end{cases} \tag{9}$$

where C_s is the specified constant for determining the system state.

When the system is operated under steady-state conditions, the performance of PLO is preferred to be with higher small signal stability. Thus, the control parameter K_P of PI-controller should have a smaller value. If CF occurs, it will be better to apply a larger K_P to gain fast dynamic response.

As depicted in Figure 6, the RMS of commutating voltage can be evaluated based on the measured three-phase voltage at the AC side. A first-order inertia link with time constant T_{rp} is firstly applied to suppress the high-frequency harmonies, followed by the derivative block to determine the signal changing rate, i.e., $\dot{U}_{rms}$. Here, T_{de} is the derivative time constant. Usually, the derivative can amplify noise, so the inertia link should be added to minimize noise interference. Then, a signal is generated by comparing $\dot{U}_{rms}$ with a specified constant C_s, shown as (9). Depending on this signal, selectors are employed to change the value of K_P and K_I.

$$\begin{cases} \text{If } \dot{U}_{rms} > C_s, K_P = K_{P1} \text{ and } K_I = K_{I1}, \\ \text{If } \dot{U}_{rms} \leq C_s, K_P = K_{P2} \text{ and } K_I = K_{I2}, \end{cases} \tag{10}$$

where K_{P1}, K_{I1}, K_{P2} and K_{I2} are different predefined gains for selectors to take.

The main idea is that K_P and K_I can be changed adaptively depending on the state of commutating voltage. In general, the RMS of the commutating voltage has its specified value ranges in many grid codes, which could be used as reference for setting Cs values. However, it is still worth noting that the setting of Cs is also a compromise between the controller's sensitivity and stability.

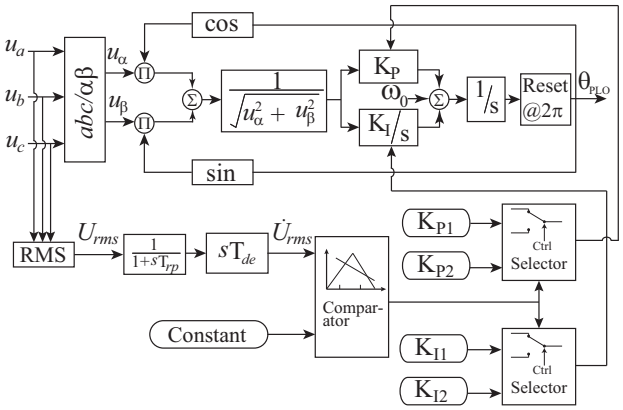

Figure 6. The adaptive PLO control block.

5. Case Studies

To investigate the effectiveness of the proposed method, the CIGRÉ benchmark model for LCC-based HVDC system is applied [21] with a short-circuit ratio of 2.0 on the platform of PSCAD/EMTDC and RT-LAB, respectively.

5.1. Three-Phase Fault

At first, simulations are performed in PSCAD/EMTDC and three phase fault is applied. The original control parameters are $K_P = 10$ and $K_I = 100$. In the proposed method, $K_{P1} = 100$, $K_{P2} = 10$, $K_{I1} = 300$ and $K_{I2} = 100$. When $t = 0.2$ s, a three-phase fault takes place at the inverter side, and the fault duration time is 0.05 s.

Figure 7 show the comparison between firing angle order and actual firing angle under the original control algorithm. At the moment of $t = 0.2$ s, commutation failure happens due to the voltage dip. After the fault is cleared, the system recovers from commutation failure. It can be seen that, the actual firing angle is greater than the firing angle order during the period between $t = 0.25$ and $t = 0.35$. That means, the measured phase angle has a time lag with the actual phase angle. From (7), the voltage-time area for commutation will be reduced, which may cause continuous commutation failures. In this case, continuous commutation failure can be observed at about $t = 0.375$ s.

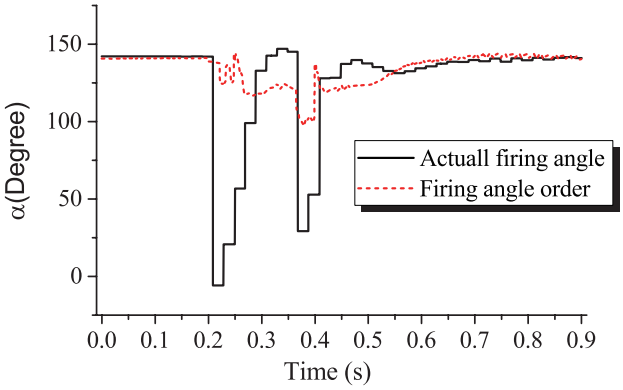

Figure 7. Comparison between the firing angle order and actual firing angle under the original control algorithm.

In Figure 8, the actual firing angle and firing angle order are compared under the proposed method. It can be seen that, the actual firing angle is almost same with the order after the fault is cleared at $t = 0.25$ s. That means the output of PLO can reflect the phase angle during the process of recovery from CF. If the control order of the system controller can be effectively implemented, continuous CF can be avoided in this case. If the original control parameters are applied, the control order cannot be carried out correctly and the unexpected continuous CF will occur. To better demonstrate the commutation

progress, the responses of extinguish angle and commutating voltage under different control algorithms are given in Figure 9 and Figure 10, respectively. It can be seen that, the proposed method can eliminate the continuous commutation failure, which will benefit the voltage recovery.

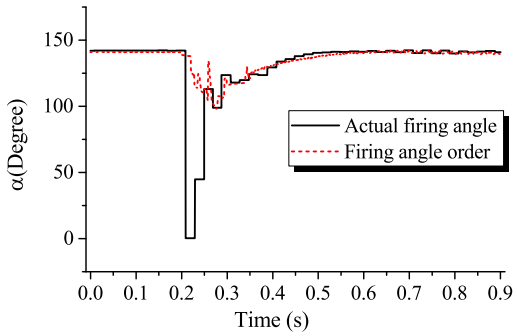

Figure 8. Comparison between the actual firing angle and firing angle order under 3PF.

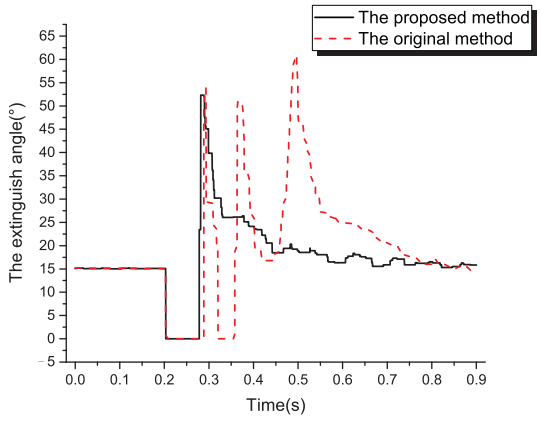

Figure 9. Comparison of extinguish angle between the proposed and original control algorithms under 3PF.

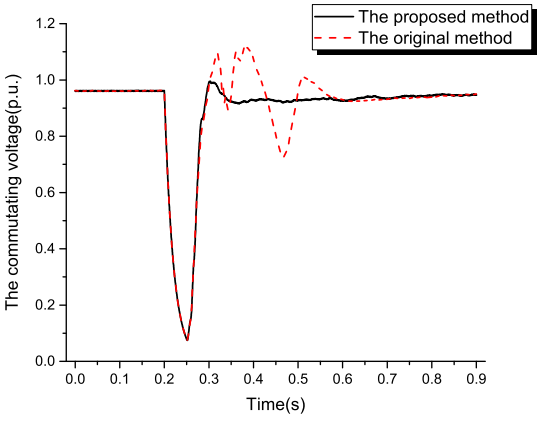

Figure 10. Comparison of commutating voltage between the proposed and original control algorithms under 3PF.

5.2. Single Phase Ground Fault

In the second case, the unbalanced fault is applied in PSCAD/EMTDC, where the control parameters are set as the same with the ones in Section 5.1. When $t = 0.2$ s, a fault happens at phase-A and is cleared after 0.1 s.

Figure 11 show the comparison under the original control algorithm. It can be seen that, the actual firing angle is less than the firing angle order during the period between $t = 0.3$ and $t = 0.35$. In this case, the voltage-time area for commutation is larger than the one expected, so no CF occurs. After that, the actual firing angle is greater than the order, which means the actual commutation area is smaller than the ordered. Thus, continuous CF takes place at the moment of $t = 0.4$ s. During the recovery process from second CF, the phase angle with time lags provided by the original PLO leads to the third CF. If the protection scheme of continuous CFs is implemented, this converter will be blocked. Compared to the case with balanced faults, the original control strategy may lead to a worse result in the case with unbalanced faults.

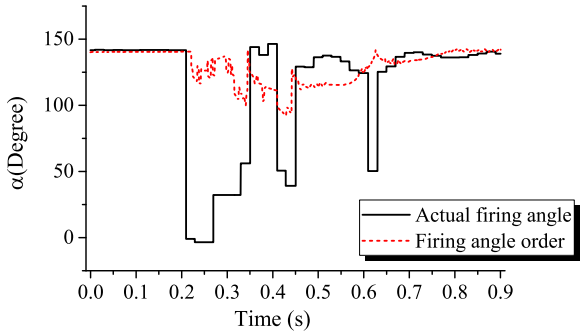

Figure 11. Comparison between the actual firing angle and firing angle order with the original algorithm under the single-line ground fault.

Compared to the original strategy, Figure 12 shows the actual firing angle and firing angle order under the proposed method. It can be seen that the firing angle order can be carried out better, and no continuous CF is observed. That means, the proposed method can enhance the ability of recovery from CF with unbalanced faults, compared to the original strategy. The response of extinguish angle and commutating voltage under different control algorithms are given in Figure 13 and Figure 14, respectively. Similar with the case under 3PF, the proposed method performs better than the original algorithm does. When $t = 0.35$ s, the extinguish angle reduce dramatically to the critical extinguish angle under the original method, meaning that a continuous commutation failure happens. On the contrary, the proposed method can capture the phase information correctly and the fault recovery performs normally under the expected strategy.

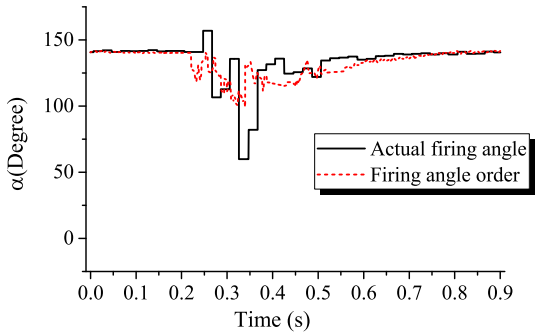

Figure 12. Comparison between the actual firing angle and firing angle order with the proposed algorithm under the single-line ground fault.

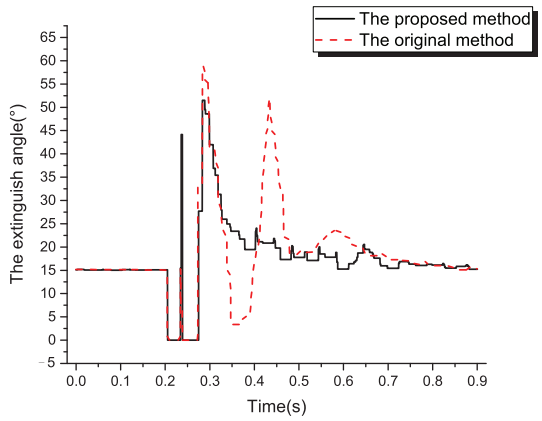

Figure 13. Comparison of extinguish angle between the proposed and original control algorithms under SLGF.

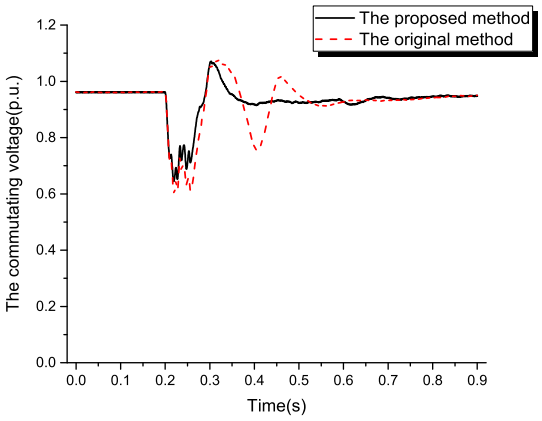

Figure 14. Comparison of commutating voltage between the proposed and original control algorithms under SLGF.

5.3. Small Signal Stability

In this case, the small signal stability of the proposed method is investigated. From Section 3.2, it is known that the parameter K_P with larger value can provide a faster response, but may make the small signal stability worse. So, if the system is operated under normal condition, the control parameters are adaptively changed to smaller ones in the proposed method. Here, we set K_P and K_I to 100 and 300 for the conventional constant control strategies, even in the normal operation while $K_{P1} = 100$, $K_{P2} = 10$, $K_{I1} = 300$ and $K_{I2} = 100$ for the proposed adaptive strategy which are the same as previous subsections. A single-line ground fault with a 400 Ω fault resistance is applied at phase-A at $t = 0.1$ s and cleared after 0.1 s. The fault resistance applied here is relative high, and commutation failure will not happen, which can be interpreted as a small disturbance to the HVDC system. A comparison of commutating voltage between the proposed method and the one with larger parameters is shown as Figure 15.

It can be seen that, the commutating voltage under the proposed method begins to stabilize at about $t = 0.35$ s , and the control parameters for normal operation will be effective at this moment. On the contrary, the voltage with larger K_P and K_I does not shift toward the stable state but fluctuates, which means the control parameters applied in the transient process of recovery may cause stability problems under small disturbance.

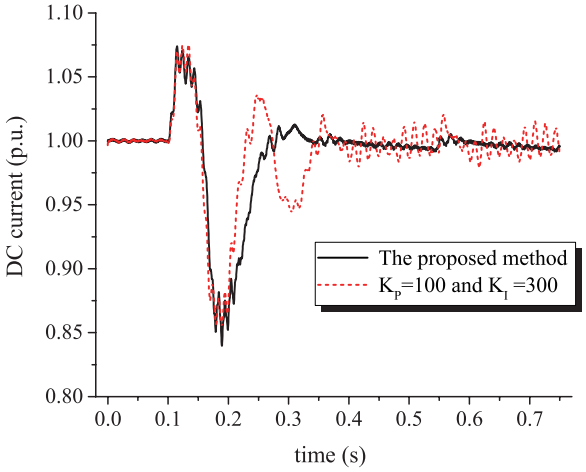

Figure 15. Stability comparison between the proposed method and the original method.

5.4. Recovery Performance Comparison with Traditional Approaches

To counter the commutation failure, one of the most popular and effective solutions is to trigger the thyristor gates in advance, which may however slow down the recovery speed. Here, the benefit of the proposed method is investigated on the platform of RT-LAB, and a comparison with the dynamic phasor-based (DP-based) PLL proposed in [16] is presented.

To investigate the performance of proposed method and its beneficial after application, a single-line ground fault with 100 Ω is applied at $t = 0.1$ s and cleared after 0.1 s. In this case, an improved CFPREV control is compared [12], where the recovery speed is limited by the commutation margin. Figure 16 illustrates the performance of firing angle order by different methods. During the fault recovery process, the firing angle order recovers faster, if the proposed PLO is used. The reason for this is that an accurate voltage phase angle can largely improve the effectiveness of the control strategy. The error of phase angle may cause an incorrect execution, so that the controller must slow down the recovery process to ensure that the recovery is successful.

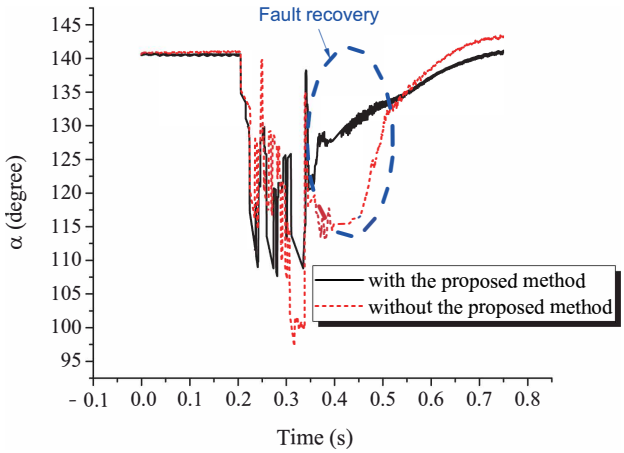

Figure 16. The firing angle order comparison after applying the proposed method.

Aside from the recovery speed, the commutation margin is also compared, and Figure 17 shows a comparison of the γ. It can be seen that, the implementation of our method can provide a better result. During the recovery process, the extinguish angle of the proposed method is maintained at about 20 degrees, whereas the result by conventional approach reaches about 15 degrees. The proposed method enhances the effectiveness of the recovery control strategy by considering both the recovery speed and the risk of failure.

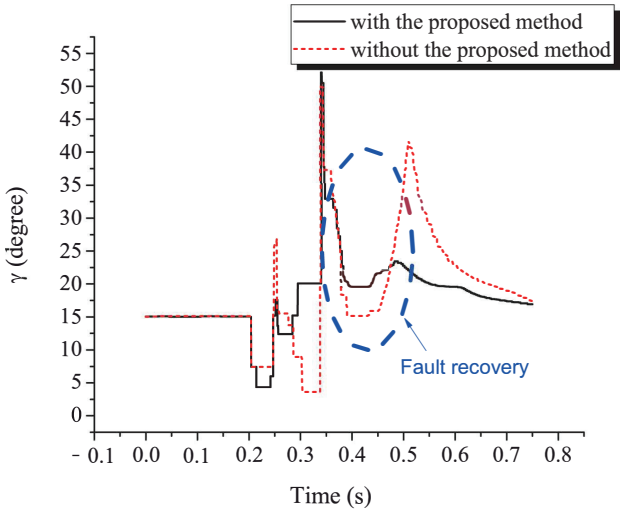

Figure 17. The extinguish angle comparison after applying the proposed method.

To further investigate the effectiveness compared with other similar techniques, a DP-based PLL is compared, which is based on the theory of Fourier expansion. Figure 18 depicts the comparison between different approaches. During the recovery process, the original PLO provides a phase angle with time lag, shown as the blue dashed line. From Section 2.2, it is known that this time lag may result in recovery failure. As for the comparison between the proposed method and DP-based approach, there is almost no difference between their results. It can be seen that the output of PLO of the proposed method and DP-based PLL are almost identical, which verifies the accuracy of our method. Although the DP-based method gains high accuracy during the large disturbance, the small signal stability should also be considered.

Figure 19 shows the small signal response comparison, where a single-line ground fault of 700 Ω is applied at phase-A when $t = 0.2$ and cleared after 0.1 s. As seen, an oscillation occurs in the results by DP-based method, whereas the oscillation of the proposed method is much better. Moreover, it should be pointed out that the proposed PLO can be realized by modifying the original control, while the DP-based approach requires a completely new implementation.

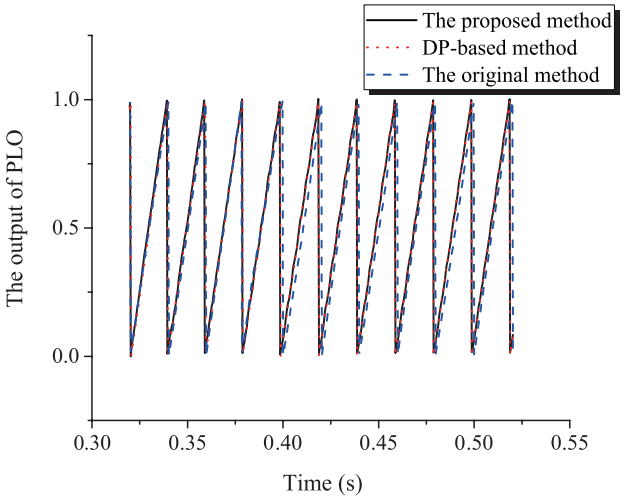

Figure 18. The PLO output comparison between different methods.

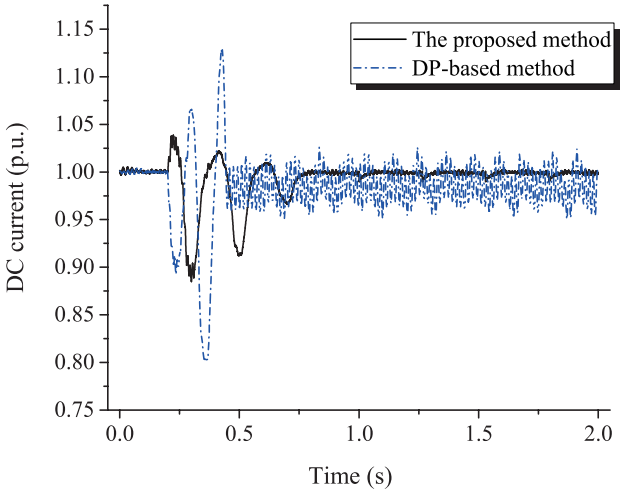

Figure 19. The stability comparison between DP-based method and the proposed method.

6. Conclusions

In this paper, an adaptive PLO scheme is proposed to enhance the recovery ability from CFs. The proposed method aims to provide phase angle information with better accuracy, where two groups of control parameters are selected according to the system state. When the system is under the recovery process from CF, the PLO tends to trace the voltage phase with a faster response. If the system is operated under normal conditions, traditional control parameters with better small single stability are chosen. Case studies show that the proposed method has better performance under both balanced faults and unbalanced faults, compared to the control strategy with constant parameters. The maximum current overshoot is reduced by approximately 50%, resulting in significant reductions in the amplitude of oscillations.

Author Contributions: H.C. and Y.Z.; methodology, Y.Z.; software, Y.H.; validation, H.C., J.L. and Y.Z.; formal analysis, Y.H.; investigation, H.C.; resources, J.L.; data curation, J.L.; writing—original draft preparation, H.C.; writing—review and editing, Y.Z.; visualization, Y.H.; supervision, J.L.; project administration, Y.Z.; funding acquisition, H.C. All authors have read and agreed to the published version of the manuscript.

Funding: This research was funded by "Pioneer" and "Leading Goose" R&D Program of Zhejiang (2022C01161).

Data Availability Statement: The data presented in this study are available on request from the corresponding author.

Conflicts of Interest: The authors declare no conflict of interest.

References

1. Thio, C.V.; Davies, J.B.; Kent, K.L. Commutation failures in HVDC transmission systems. *IEEE Trans. Power Deliv.* **1996**, *11*, 946–957. [CrossRef]
2. Wang, Q.; Zhang, C.; Wu, X.; Tang, Y. Commutation Failure Prediction Method Considering Commutation Voltage Distortion and DC Current Variation. *IEEE Access* **2019**, *7*, 96531–96539. [CrossRef]
3. Cheng, J.; Xue, Y.; Guan, M.; Wang, C. Analysis of the commutation failure of inverters during open-conductor faults at the AC side. *Int. Trans. Electr. Energy Syst.* **2015**, *25*, 1570–1589. [CrossRef]
4. Guo, Q.; Yoon, M.; Kim, C.; Jang, G. Commutation failure and voltage sensitivity analysis in a hybrid multi-infeed HVDC system containing modular multilevel converter. *Int. Trans. Electr. Energy Syst.* **2016**, *26*, 2259–2271. [CrossRef]
5. Zhang, G.; Jing, L.; Liu, M.; Wang, B.; Dong, X. An Improved Continuous Commutation Failure Mitigation Method in High Voltage Direct Current Transmission System. In Proceedings of the 2018 China International Conference on Electricity Distribution (CICED), Tianjin, China, 17–19 September 2018; pp. 1132–1136. [CrossRef]
6. Zhou, Y.; Wu, H.; Song, Y.; Ling, W.; Lou, B.; Deng, H. Analyses of static and dynamic reactive power allocation between synchronous compensators and shunt capacitors to counter commutation failures. *Int. Trans. Electr. Energy Syst.* **2018**, *28*, e2605. [CrossRef]

7. Liu, L.; Lin, S.; Sun, P.; Liao, K.; Li, X.; Deng, Y.; He, Z. A Calculation Method of Pseudo Extinction Angle for Commutation Failure Mitigation in HVDC. *IEEE Trans. Power Deliv.* **2019**, *34*, 777–779. [CrossRef]
8. Du, Z.; Wang, Z.; Ding, J.; Wu, C. Influence of Load Models on Commutation Failure in HVDC Transmission Systems. In Proceedings of the 2018 2nd IEEE Conference on Energy Internet and Energy System Integration (EI2), Beijing, China, 20–22 October 2018. [CrossRef]
9. Wang, C.; Zhang, C.; Kong, X.; Li, P.; Yuan, Y. Procedure analysis of UHVDC commutation failure. *J. Eng.* **2019**, *2019*, 3132–3134. [CrossRef]
10. Bauman, J.; Kazerani, M. Commutation Failure Reduction in HVDC Systems Using Adaptive Fuzzy Logic Controller. *IEEE Trans. Power Syst.* **2007**, *22*, 1995–2002. [CrossRef]
11. Wang, S.; Lu, S.; Hou, Y.; Liu, F.; Xu, Z. Improvement of HVDC commutation failure response based on compound phase-shifting control. *J. Eng.* **2017**, *2017*, 1473–1477. [CrossRef]
12. Wei, Z.; Yuan, Y.; Lei, X.; Wang, H.; Sun, G.; Sun, Y. Direct-Current Predictive Control Strategy for Inhibiting Commutation Failure in HVDC Converter. *IEEE Trans. Power Syst.* **2014**, *29*, 2409–2417. [CrossRef]
13. Zheng, Q.; Wang, X.; Fu, Y.; Yan, H.; Ou, Z.; Wang, G.; Wang, Y. A STATCOM compensation scheme for suppressing commutation failure in HVDC. In Proceedings of the IECON 2016—42nd Annual Conference of the IEEE Industrial Electronics Society, Florence, Italy, 23–26 October 2016; pp. 1081–1086. [CrossRef]
14. Rehman, A.U.; Zhao, C.; Guo, C. Coordinated Control Strategy for Transient Performance Improvement of LCC Based HVDC Transmission System with STATCOM Under Weak AC Grid. In Proceedings of the 2018 2nd IEEE Conference on Energy Internet and Energy System Integration (EI2), Beijing, China, 20–22 October 2018. [CrossRef]
15. Das, B.P.; Watson, N.; Liu, Y. Simulation study of conventional and hybrid HVDC rectifier based on CIGRÉ benchmark model using PLL-less synchronisation scheme. In Proceedings of the 2011 5th International Power Engineering and Optimization Conference, Shah Alam, Malaysia, 6–7 June 2011; pp. 312–317. [CrossRef]
16. Vandaei, A.B.; Filizadeh, S.; Mudunkotuwa, K.; Tara, E. Real-time implementation of an enhanced dynamic phasor-based three-phase phase-locked loop for line-commutated converters. In Proceedings of the 2018 IEEE International Conference on Industrial Technology (ICIT), Lyon, France, 20–22 February 2018; pp. 812–817. [CrossRef]
17. Zheng, A.; Guo, C.; Cui, P.; Jiang, W.; Zhao, C. Comparative Study on Small-Signal Stability of LCC-HVDC System With Different Control Strategies at the Inverter Station. *IEEE Access* **2019**, *7*, 34946–34953. [CrossRef]
18. Kaya, S.; Alişar, İ.; Gök, G. Advanced PLL structure for HVDC transmission under unbalanced grid conditions. In Proceedings of the 2018 6th International Istanbul Smart Grids and Cities Congress and Fair (ICSG), Istanbul, Turkey, 25–26 April 2018; pp. 197–202. [CrossRef]
19. Meah, K.; Sadrul Ula, A. Simulation study of the CIGRE HVDC benchmark model with the WSCC nine-bus power system network. In Proceedings of the 2009 IEEE/PES Power Systems Conference and Exposition, Seattle, WA, USA, 15–18 March 2009; pp. 1–5. [CrossRef]
20. Szechtman, M.; Wess, T.; Thio, C. A benchmark model for HVDC system studies. In Proceedings of the International Conference on AC and DC Power Transmission, London, UK, 17–20 September 1991; pp. 374–378.
21. Mazouz, L.; Zidi, S.A.; Hafaifa, A.; Hadjeri, S.; Khatir, M.; Brahimi, L. Effect of commutation failures in a GIGRE model for HVDC link connected to AC network. In Proceedings of the 2018 International Conference on Applied Smart Systems (ICASS), Médéa, Algeria, 24–25 November 2018; pp. 1–6. [CrossRef]